Contents lists available at SciVerse ScienceDirect

Physics Letters B

www.elsevier.com/locate/physletb

Measurement of the $t\bar{t}$ production cross section using dilepton events in $p\bar{p}$ collisions

D0 Collaboration

V.M. Abazov [ai], B. Abbott [bu], B.S. Acharya [ac], M. Adams [aw], T. Adams [au], G.D. Alexeev [ai], G. Alkhazov [am], A. Alton [bi,1], G. Alverson [bh], G.A. Alves [b], L.S. Ancu [ah], M. Aoki [av], M. Arov [bf], A. Askew [au], B. Åsman [ao], O. Atramentov [bm], C. Avila [h], J. BackusMayes [cb], F. Badaud [m], L. Bagby [av], B. Baldin [av], D.V. Bandurin [au], S. Banerjee [ac], E. Barberis [bh], P. Baringer [bd], J. Barreto [c], J.F. Bartlett [av], U. Bassler [r], V. Bazterra [aw], S. Beale [f], A. Bean [bd], M. Begalli [c], M. Begel [bs], C. Belanger-Champagne [ao], L. Bellantoni [av], S.B. Beri [aa], G. Bernardi [q], R. Bernhard [v], I. Bertram [ap], M. Besançon [r], R. Beuselinck [aq], V.A. Bezzubov [al], P.C. Bhat [av], V. Bhatnagar [aa], G. Blazey [ax], S. Blessing [au], K. Bloom [bl], A. Boehnlein [av], D. Boline [br], E.E. Boos [ak], G. Borissov [ap], T. Bose [bg], A. Brandt [bx], O. Brandt [w], R. Brock [bj], G. Brooijmans [bp], A. Bross [av], D. Brown [q], J. Brown [q], X.B. Bu [av], M. Buehler [ca], V. Buescher [x], V. Bunichev [ak], S. Burdin [ap,2], T.H. Burnett [cb], C.P. Buszello [ao], B. Calpas [o], E. Camacho-Pérez [af], M.A. Carrasco-Lizarraga [bd], B.C.K. Casey [av], H. Castilla-Valdez [af], S. Chakrabarti [br], D. Chakraborty [ax], K.M. Chan [bb], A. Chandra [bz], G. Chen [bd], S. Chevalier-Théry [r], D.K. Cho [bw], S.W. Cho [ae], S. Choi [ae], B. Choudhary [ab], S. Cihangir [av], D. Claes [bl], J. Clutter [bd], M. Cooke [av], W.E. Cooper [av], M. Corcoran [bz], F. Couderc [r], M.-C. Cousinou [o], A. Croc [r], D. Cutts [bw], A. Das [as], G. Davies [aq], K. De [bx], S.J. de Jong [ah], E. De La Cruz-Burelo [af], F. Déliot [r], M. Demarteau [av], R. Demina [bq], D. Denisov [av], S.P. Denisov [al], S. Desai [av], C. Deterre [r], K. DeVaughan [bl], H.T. Diehl [av], M. Diesburg [av], A. Dominguez [bl], T. Dorland [cb], A. Dubey [ab], L.V. Dudko [ak], D. Duggan [bm], A. Duperrin [o], S. Dutt [aa], A. Dyshkant [ax], M. Eads [bl], D. Edmunds [bj], J. Ellison [at], V.D. Elvira [av], Y. Enari [q], H. Evans [az], A. Evdokimov [bs], V.N. Evdokimov [al], G. Facini [bh], T. Ferbel [bq], F. Fiedler [x], F. Filthaut [ah], W. Fisher [bj], H.E. Fisk [av], M. Fortner [ax], H. Fox [ap], S. Fuess [av], A. Garcia-Bellido [bq], V. Gavrilov [aj], P. Gay [m], W. Geng [o,bj], D. Gerbaudo [bn], C.E. Gerber [aw], Y. Gershtein [bm], G. Ginther [av,bq], G. Golovanov [ai], A. Goussiou [cb], P.D. Grannis [br], S. Greder [s], H. Greenlee [av], Z.D. Greenwood [bf], E.M. Gregores [d], G. Grenier [t], Ph. Gris [m], J.-F. Grivaz [p], A. Grohsjean [r], S. Grünendahl [av], M.W. Grünewald [ad], T. Guillemin [p], F. Guo [br], G. Gutierrez [av], P. Gutierrez [bu], A. Haas [bp,3], S. Hagopian [au], J. Haley [bh], L. Han [g], K. Harder [ar], A. Harel [bq], J.M. Hauptman [bc], J. Hays [aq], T. Head [ar], T. Hebbeker [u], D. Hedin [ax], H. Hegab [bv], A.P. Heinson [at], U. Heintz [bw], C. Hensel [w], I. Heredia-De La Cruz [af], K. Herner [bi], G. Hesketh [ar,4], M.D. Hildreth [bb], R. Hirosky [ca], T. Hoang [au], J.D. Hobbs [br], B. Hoeneisen [l], M. Hohlfeld [x], Z. Hubacek [j,r], N. Huske [q], V. Hynek [j], I. Iashvili [bo], R. Illingworth [av], A.S. Ito [av], S. Jabeen [bw], M. Jaffré [p], D. Jamin [o], A. Jayasinghe [bu], R. Jesik [aq], K. Johns [as], M. Johnson [av], D. Johnston [bl], A. Jonckheere [av], P. Jonsson [aq], J. Joshi [aa], A.W. Jung [av], A. Juste [an], K. Kaadze [be], E. Kajfasz [o], D. Karmanov [ak], P.A. Kasper [av], I. Katsanos [bl], R. Kehoe [by], S. Kermiche [o], N. Khalatyan [av], A. Khanov [bv], A. Kharchilava [bo], Y.N. Kharzheev [ai], D. Khatidze [bw], M.H. Kirby [ay], J.M. Kohli [aa], A.V. Kozelov [al], J. Kraus [bj], S. Kulikov [al], A. Kumar [bo], A. Kupco [k], T. Kurča [t], V.A. Kuzmin [ak], J. Kvita [i], S. Lammers [az], G. Landsberg [bw], P. Lebrun [t], H.S. Lee [ae], S.W. Lee [bc], W.M. Lee [av], J. Lellouch [q], L. Li [at], Q.Z. Li [av], S.M. Lietti [e], J.K. Lim [ae], D. Lincoln [av], J. Linnemann [bj], V.V. Lipaev [al], R. Lipton [av], Y. Liu [g], Z. Liu [f], A. Lobodenko [am], M. Lokajicek [k], R. Lopes de Sa [br], H.J. Lubatti [cb], R. Luna-Garcia [af,5], A.L. Lyon [av], A.K.A. Maciel [b], D. Mackin [bz], R. Madar [r], R. Magaña-Villalba [af], S. Malik [bl], V.L. Malyshev [ai], Y. Maravin [be], J. Martínez-Ortega [af], R. McCarthy [br], C.L. McGivern [bd], M.M. Meijer [ah], A. Melnitchouk [bk], D. Menezes [ax], P.G. Mercadante [d], M. Merkin [ak], A. Meyer [u], J. Meyer [w], F. Miconi [s], N.K. Mondal [ac], G.S. Muanza [o], M. Mulhearn [ca], E. Nagy [o],

M. Naimuddin [ab], M. Narain [bw], R. Nayyar [ab], H.A. Neal [bi], J.P. Negret [h], P. Neustroev [am], S.F. Novaes [e],
T. Nunnemann [y], G. Obrant [am], J. Orduna [bz], N. Osman [o], J. Osta [bb], G.J. Otero y Garzón [a], M. Padilla [at],
A. Pal [bx], N. Parashar [ba], V. Parihar [bw], S.K. Park [ae], J. Parsons [bp], R. Partridge [bw,3], N. Parua [az], A. Patwa [bs],
B. Penning [av], M. Perfilov [ak], K. Peters [ar], Y. Peters [ar], K. Petridis [ar], G. Petrillo [bq], P. Pétroff [p], R. Piegaia [a],
J. Piper [bj], M.-A. Pleier [bs], P.L.M. Podesta-Lerma [af,6], V.M. Podstavkov [av], P. Polozov [aj], A.V. Popov [al],
M. Prewitt [bz], D. Price [az], N. Prokopenko [al], S. Protopopescu [bs], J. Qian [bi], A. Quadt [w], B. Quinn [bk],
M.S. Rangel [b], K. Ranjan [ab], P.N. Ratoff [ap], I. Razumov [al], P. Renkel [by], M. Rijssenbeek [br], I. Ripp-Baudot [s],
F. Rizatdinova [bv], M. Rominsky [av], A. Ross [ap], C. Royon [r], P. Rubinov [av], R. Ruchti [bb], G. Safronov [aj],
G. Sajot [n], P. Salcido [ax], A. Sánchez-Hernández [af], M.P. Sanders [y], B. Sanghi [av], A.S. Santos [e], G. Savage [av],
L. Sawyer [bf], T. Scanlon [aq], R.D. Schamberger [br], Y. Scheglov [am], H. Schellman [ay], T. Schliephake [z],
S. Schlobohm [cb], C. Schwanenberger [ar], R. Schwienhorst [bj], J. Sekaric [bd], H. Severini [bu], E. Shabalina [w],
V. Shary [r], A.A. Shchukin [al], R.K. Shivpuri [ab], V. Simak [j], V. Sirotenko [av], P. Skubic [bu], P. Slattery [bq],
D. Smirnov [bb], K.J. Smith [bo], G.R. Snow [bl], J. Snow [bt], S. Snyder [bs], S. Söldner-Rembold [ar], L. Sonnenschein [u],
K. Soustruznik [i], J. Stark [n], V. Stolin [aj], D.A. Stoyanova [al], M. Strauss [bu], D. Strom [aw], L. Stutte [av], L. Suter [ar],
P. Svoisky [bu], M. Takahashi [ar], A. Tanasijczuk [a], W. Taylor [f], M. Titov [r], V.V. Tokmenin [ai], Y.-T. Tsai [bq],
D. Tsybychev [br], B. Tuchming [r], C. Tully [bn], L. Uvarov [am], S. Uvarov [am], S. Uzunyan [ax], R. Van Kooten [az],
W.M. van Leeuwen [ag], N. Varelas [aw], E.W. Varnes [as], I.A. Vasilyev [al], P. Verdier [t], L.S. Vertogradov [ai],
M. Verzocchi [av], M. Vesterinen [ar], D. Vilanova [r], P. Vokac [j], H.D. Wahl [au], M.H.L.S. Wang [bq], J. Warchol [bb],
G. Watts [cb], M. Wayne [bb], M. Weber [av,7], L. Welty-Rieger [ay], A. White [bx], D. Wicke [z], M.R.J. Williams [ap],
G.W. Wilson [bd], M. Wobisch [bf], D.R. Wood [bh], T.R. Wyatt [ar], Y. Xie [av], C. Xu [bi], S. Yacoob [ay], R. Yamada [av],
W.-C. Yang [ar], T. Yasuda [av], Y.A. Yatsunenko [ai], Z. Ye [av], H. Yin [av], K. Yip [bs], S.W. Youn [av], J. Yu [bx],
S. Zelitch [ca], T. Zhao [cb], B. Zhou [bi], J. Zhu [bi], M. Zielinski [bq], D. Zieminska [az], L. Zivkovic [bw]

[a] *Universidad de Buenos Aires, Buenos Aires, Argentina*
[b] *LAFEX, Centro Brasileiro de Pesquisas Físicas, Rio de Janeiro, Brazil*
[c] *Universidade do Estado do Rio de Janeiro, Rio de Janeiro, Brazil*
[d] *Universidade Federal do ABC, Santo André, Brazil*
[e] *Instituto de Física Teórica, Universidade Estadual Paulista, São Paulo, Brazil*
[f] *Simon Fraser University, Vancouver, British Columbia, and York University, Toronto, Ontario, Canada*
[g] *University of Science and Technology of China, Hefei, People's Republic of China*
[h] *Universidad de los Andes, Bogotá, Colombia*
[i] *Charles University, Faculty of Mathematics and Physics, Center for Particle Physics, Prague, Czech Republic*
[j] *Czech Technical University in Prague, Prague, Czech Republic*
[k] *Center for Particle Physics, Institute of Physics, Academy of Sciences of the Czech Republic, Prague, Czech Republic*
[l] *Universidad San Francisco de Quito, Quito, Ecuador*
[m] *LPC, Université Blaise Pascal, CNRS/IN2P3, Clermont, France*
[n] *LPSC, Université Joseph Fourier Grenoble 1, CNRS/IN2P3, Institut National Polytechnique de Grenoble, Grenoble, France*
[o] *CPPM, Aix-Marseille Université, CNRS/IN2P3, Marseille, France*
[p] *LAL, Université Paris-Sud, CNRS/IN2P3, Orsay, France*
[q] *LPNHE, Universités Paris VI and VII, CNRS/IN2P3, Paris, France*
[r] *CEA, Irfu, SPP, Saclay, France*
[s] *IPHC, Université de Strasbourg, CNRS/IN2P3, Strasbourg, France*
[t] *IPNL, Université Lyon 1, CNRS/IN2P3, Villeurbanne, France and Université de Lyon, Lyon, France*
[u] *III. Physikalisches Institut A, RWTH Aachen University, Aachen, Germany*
[v] *Physikalisches Institut, Universität Freiburg, Freiburg, Germany*
[w] *II. Physikalisches Institut, Georg-August-Universität Göttingen, Göttingen, Germany*
[x] *Institut für Physik, Universität Mainz, Mainz, Germany*
[y] *Ludwig-Maximilians-Universität München, München, Germany*
[z] *Fachbereich Physik, Bergische Universität Wuppertal, Wuppertal, Germany*
[aa] *Panjab University, Chandigarh, India*
[ab] *Delhi University, Delhi, India*
[ac] *Tata Institute of Fundamental Research, Mumbai, India*
[ad] *University College Dublin, Dublin, Ireland*
[ae] *Korea Detector Laboratory, Korea University, Seoul, Republic of Korea*
[af] *CINVESTAV, Mexico City, Mexico*
[ag] *FOM – Institute NIKHEF and University of Amsterdam/NIKHEF, Amsterdam, The Netherlands*
[ah] *Radboud University Nijmegen/NIKHEF, Nijmegen, The Netherlands*
[ai] *Joint Institute for Nuclear Research, Dubna, Russia*
[aj] *Institute for Theoretical and Experimental Physics, Moscow, Russia*
[ak] *Moscow State University, Moscow, Russia*
[al] *Institute for High Energy Physics, Protvino, Russia*
[am] *Petersburg Nuclear Physics Institute, St. Petersburg, Russia*
[an] *Institució Catalana de Recerca i Estudis Avançats (ICREA) and Institut de Física d'Altes Energies (IFAE), Barcelona, Spain*
[ao] *Stockholm University, Stockholm and Uppsala University, Uppsala, Sweden*
[ap] *Lancaster University, Lancaster LA1 4YB, United Kingdom*
[aq] *Imperial College London, London SW7 2AZ, United Kingdom*
[ar] *The University of Manchester, Manchester M13 9PL, United Kingdom*
[as] *University of Arizona, Tucson, AZ 85721, USA*

[at] *University of California Riverside, Riverside, CA 92521, USA*
[au] *Florida State University, Tallahassee, FL 32306, USA*
[av] *Fermi National Accelerator Laboratory, Batavia, IL 60510, USA*
[aw] *University of Illinois at Chicago, Chicago, IL 60607, USA*
[ax] *Northern Illinois University, DeKalb, IL 60115, USA*
[ay] *Northwestern University, Evanston, IL 60208, USA*
[az] *Indiana University, Bloomington, IN 47405, USA*
[ba] *Purdue University Calumet, Hammond, IN 46323, USA*
[bb] *University of Notre Dame, Notre Dame, IN 46556, USA*
[bc] *Iowa State University, Ames, IA 50011, USA*
[bd] *University of Kansas, Lawrence, KS 66045, USA*
[be] *Kansas State University, Manhattan, KS 66506, USA*
[bf] *Louisiana Tech University, Ruston, LA 71272, USA*
[bg] *Boston University, Boston, MA 02215, USA*
[bh] *Northeastern University, Boston, MA 02115, USA*
[bi] *University of Michigan, Ann Arbor, MI 48109, USA*
[bj] *Michigan State University, East Lansing, MI 48824, USA*
[bk] *University of Mississippi, University, MS 38677, USA*
[bl] *University of Nebraska, Lincoln, NE 68588, USA*
[bm] *Rutgers University, Piscataway, NJ 08855, USA*
[bn] *Princeton University, Princeton, NJ 08544, USA*
[bo] *State University of New York, Buffalo, NY 14260, USA*
[bp] *Columbia University, New York, NY 10027, USA*
[bq] *University of Rochester, Rochester, NY 14627, USA*
[br] *State University of New York, Stony Brook, NY 11794, USA*
[bs] *Brookhaven National Laboratory, Upton, NY 11973, USA*
[bt] *Langston University, Langston, OK 73050, USA*
[bu] *University of Oklahoma, Norman, OK 73019, USA*
[bv] *Oklahoma State University, Stillwater, OK 74078, USA*
[bw] *Brown University, Providence, RI 02912, USA*
[bx] *University of Texas, Arlington, TX 76019, USA*
[by] *Southern Methodist University, Dallas, TX 75275, USA*
[bz] *Rice University, Houston, TX 77005, USA*
[ca] *University of Virginia, Charlottesville, VA 22901, USA*
[cb] *University of Washington, Seattle, WA 98195, USA*

A R T I C L E   I N F O

A B S T R A C T

We present a measurement of the $t\bar{t}$ production cross section $\sigma_{t\bar{t}}$ in $p\bar{p}$ collisions at $\sqrt{s} = 1.96$ TeV using 5.4 fb^{-1} of integrated luminosity collected with the D0 detector. We consider final states with at least two jets and two leptons (ee, $e\mu$, $\mu\mu$), and events with one jet for the $e\mu$ final state as well. The measured cross section is $\sigma_{t\bar{t}} = 7.36^{+0.90}_{-0.79}$(stat + syst) pb. This result combined with the cross section measurement in the lepton + jets final state yields $\sigma_{t\bar{t}} = 7.56^{+0.63}_{-0.56}$(stat + syst) pb, which agrees with the standard model expectation. The relative precision of 8% of this measurement is comparable to the precision of the latest theoretical calculations.

1. Introduction

The precise measurement of the top quark pair ($t\bar{t}$) production cross section ($\sigma_{t\bar{t}}$) and its comparison with the theoretical predictions provide important tests of perturbative quantum chromodynamics (QCD). At present, the most precise predictions of $\sigma_{t\bar{t}}$ are given by approximate next to next-to-leading order (NNLO) calculations [1–3], that set a goal for the experimental precision of the $\sigma_{t\bar{t}}$ measurement of (6–9)%. Furthermore, because $\sigma_{t\bar{t}}$ depends on the top quark mass (m_t), it can be used to measure m_t [4,5]. Comparing the standard model (SM) prediction with the measured $\sigma_{t\bar{t}}$ value allows testing for the presence of physics beyond the SM, for instance, scenarios in which the top quark would decay into a charged Higgs boson and a b quark [5].

In this Letter we present an updated measurement of $\sigma_{t\bar{t}}$ in $p\bar{p}$ collisions at $\sqrt{s} = 1.96$ TeV in the dilepton ($\ell\ell'$, $\ell = e, \mu$) channel. Within the SM, top quarks decay almost 100% of the time into a W boson and a b quark. We consider the leptonic decays of both W bosons from top quark decay into $e\nu_e$, $\mu\nu_\mu$, or $\tau\nu_\tau$ (throughout this Letter, e, μ, τ refer to both charge conjugate states: $e^\pm$, $\mu^\pm$ or $\tau^\pm$), where only leptonic decays of the τ are considered.

This measurement complements the $\sigma_{t\bar{t}}$ measurements in the lepton + jets (ℓj) channel, in which one of the W bosons decays hadronically into a $q\bar{q}'$ pair and the other W boson decays leptonically [6,7], as well as measurements in the all-hadronic channel, in which both W bosons decay hadronically [8].

The measurement is based on data collected with the D0 detector during Run II of the Fermilab Tevatron Collider that correspond to an integrated luminosity of 5.4 ± 0.3 fb^{-1}. This result supersedes our previous measurement [9], which used a dataset five times smaller than the one considered here. The CDF Collaboration has measured $\sigma_{t\bar{t}}$ in the $\ell\ell'$ channel using 2.8 fb^{-1} of integrated luminosity [10]. The ATLAS and CMS Collaborations

1 Visitor from Augustana College, Sioux Falls, SD, USA.
2 Visitor from The University of Liverpool, Liverpool, UK.
3 Visitor from SLAC, Menlo Park, CA, USA.
4 Visitor from University College London, London, UK.
5 Visitor from Centro de Investigacion en Computacion – IPN, Mexico City, Mexico.
6 Visitor from ECFM, Universidad Autonoma de Sinaloa, Culiacán, Mexico.
7 Visitor from Universität Bern, Bern, Switzerland.

recently published their first $\sigma_{t\bar{t}}$ measurements in pp collisions at $\sqrt{s} = 7$ TeV [11,12].

The D0 detector is described in detail in [13]. The region of the D0 detector closest to the interaction region contains a tracking system consisting of a silicon microstrip tracker and a central fiber tracker, both located inside a superconducting solenoid magnet which generates a magnetic field of 2 T. Hits in these two detectors are used to reconstruct tracks from charged particles in the pseudorapidity region $|\eta| < 3$.[8] Surrounding the two tracking subdetectors are liquid-argon uranium calorimeters, segmented into electromagnetic and hadronic sections. The central section of the calorimeter (CC) covers pseudorapidities $|\eta| < 1.1$, and the two end calorimeters (EC) extend coverage to $|\eta| \approx 4.2$ with all three housed in separate cryostats. The muon system surrounds the calorimeter and consists of three layers of tracking detectors and scintillator trigger counters covering $|\eta| < 2$. A toroidal iron magnet with a field of 1.8 T is located outside the innermost layer of the muon detector. The luminosity is calculated from the rate of inelastic $p\bar{p}$ collisions measured with plastic scintillator arrays located in front of the EC cryostats [14].

The D0 trigger is based on a three-level pipeline system. The first level is implemented in custom-designed hardware. The second level uses high-level processors to combine information from the different sub-detectors to construct simple physics objects. The software-based third level uses full event information obtained with a simplified reconstruction algorithm.

2. Object identification

The $t\bar{t}$ dilepton final state contains two leptons (electrons, muons or an electron and a muon), at least two jets, and significant missing transverse momentum ($\not{p}_T$) from escaping neutrinos.

Electrons are identified as energy clusters with radius $\mathcal{R} = \sqrt{(\Delta\eta)^2 + (\Delta\phi)^2} < 0.2$ in the calorimeter (ϕ is the azimuthal angle) which are consistent in their longitudinal and transverse profiles with those of an electromagnetic shower. More than 90% of the energy of the electron candidate must be deposited in the electromagnetic part of the calorimeter, and less than 20% of its energy may be deposited in an annulus of $0.2 < \mathcal{R} < 0.4$ around its direction. This cluster has to be matched to an inner detector track. We consider electrons in the CC with $|\eta| < 1.1$ and in the EC with $1.5 < |\eta| < 2.5$. In addition, we make a requirement on the electron likelihood discriminant, based on tracking and calorimeter information, at a cut value chosen to have a high selection efficiency (near 85%) for electrons, and good rejection (near 90%) for jets misidentified as electrons. Electrons fulfilling all these criteria are called "tight electrons".

A muon is identified as a segment in at least one layer of the muon system in the full acceptance of the muon system that is matched to a track in the central tracking system. Reconstructed muons must satisfy two isolation criteria. First, the transverse energy deposited in an annulus around the muon $0.1 < \mathcal{R} < 0.4$ ($E_T^{\mu,\mathrm{iso}}$) has to be less than 15% of the transverse momentum of the muon (p_T^μ). Second, the sum of the transverse momenta of the tracks in a cone of radius $\mathcal{R} < 0.5$ around the muon track in the central tracking system ($p_T^{\mu,\mathrm{iso}}$) has to be less than 15% of p_T^μ. Muons that fulfill these isolation criteria are referred to as "tight isolated muons".

Monte Carlo (MC) generated events are processed through a GEANT3 [15] based simulation of the D0 detector and the same re-

construction programs used for the data. To simulate the effects from additional $p\bar{p}$ interactions, zero bias events with no trigger requirements selected randomly in collider data are overlayed on the fully simulated MC events. Residual differences between data and MC simulation in the electron and muon p_T resolutions and identification efficiencies are corrected. These corrections are derived from a sample of $Z/\gamma^\star \rightarrow \ell\ell$ events in data and MC, applying tight requirements on one of the two leptons for selecting the events and using the other one to measure the efficiencies and resolutions.

Jets are identified with a cone algorithm with radius $\mathcal{R} < 0.5$ [16] in the range $|\eta| < 2.5$. A jet energy scale correction (JES) is determined by calibrating the energy deposited in the jet cone using transverse momentum balance in $\gamma + $ jet and dijet events. If a muon overlaps with the jet cone, the momentum of that muon is added to the jet p_T, assuming that the muon originates from a semileptonic decay of a hadron belonging to the jet.

We require that the jets be matched to at least two tracks originating from the vertex of the primary $p\bar{p}$ interaction (PV). Jets in MC are corrected for the residual differences between data and MC in the energy resolution and JES. These correction factors are measured by comparing data and MC in $(Z/\gamma^\star \rightarrow ee) + $ jets events.

We use a neural-network (NN) tagging algorithm [17] to identify jets from b quarks. The algorithm combines information from the impact parameters of the tracks and variables that characterize the presence and properties of secondary vertices within the jet in a single discriminant. In order to use this information for b tagging, the jet is required to be matched to a jet built from tracks. Jets fulfilling this requirement are called taggable jets. The NN discriminant has a value close to one for the b quark jets and close to zero for the light quark and gluon jets.

The $\not{p}_T$ is reconstructed from the energy deposited in the calorimeter cells. Corrections for lepton and jet p_T are propagated into the $\not{p}_T$. The missing transverse momentum significance ($\sigma_{\not{p}_T}$) is defined in each event as a likelihood discriminant constructed using the ratio of $\not{p}_T$ to its uncertainty.

More details about object identification can be found in [18].

3. Event selection and background estimation

The main sources of background in the $\ell\ell'$ channel come from Drell–Yan and Z boson production ($Z/\gamma^\star \rightarrow \ell\ell$), diboson production ($WW$, WZ, ZZ), and instrumental background. The instrumental background mainly arises from multijet and $(W \rightarrow \ell\nu) + $ jets events in which one or two jets are misidentified as electrons and/or muons originating from the semileptonic decay of a heavy flavor hadron.

For this analysis we consider events that passed at least one of a set of single lepton triggers for the ee and $\mu\mu$ channels. For the $e\mu$ channel, we consider events selected by a mixture of single and multilepton triggers and lepton + jet triggers. Efficiencies for single lepton triggers have been measured with $Z/\gamma^\star \rightarrow \ell\ell$ data. These efficiencies are found to be around 99% for the ee channel and 80% for $\mu\mu$. For the $e\mu$ channel the trigger efficiency is close to 100%.

In order to separate $t\bar{t}$ signal events from background, the following selection is applied:

- We require at least one PV in the beam interaction region with $|z| < 60$ cm, where z is the coordinate along the beam axis, and $z = 0$ in the center of the detector. At least three tracks must be associated with this PV.
- We require at least two isolated leptons with $p_T > 15$ GeV, originating from the same PV, i.e., the difference between the z coordinates of the two lepton tracks should be less than 2 cm,

---

[8] The pseudorapidity is defined as $\eta = -\ln[\tan(\theta/2)]$, where θ is the polar angle with respect to the proton beam.

where the z coordinate is calculated at the point of the track's closest approach to the beam.

- We select the two highest p_T leptons with opposite charges.
- In the $e\mu$ final state, we require the distance between the electron and the muon directions to be $R(e, \mu) > 0.3$ to reduce the background from bremsstrahlung.
- In the $e\mu$ channel, we consider events with at least one jet with $p_T > 20$ GeV. In the ee and $\mu\mu$ channels, we require at least two jets with $p_T > 20$ GeV.
- To further improve the signal purity of the selected sample, we apply additional selection criteria based on global event properties. In the $e\mu$ channel with exactly one jet, we require $H_T > 105$ GeV, where H_T is the scalar sum of the transverse momenta of the leading lepton and the two leading jets. In the $e\mu$ final state with two jets, we require $H_T > 110$ GeV. In the ee final state, we require $\sigma_{\not{p}_T} > 5$, while in the $\mu\mu$ channel we require $\not{p}_T > 40$ GeV and $\sigma_{\not{p}_T} > 5$.

In order to estimate the signal efficiency and the background contamination, we use the MC simulation for all contributions but for the instrumental background, the latter being derived from data. The $t\bar{t}$ and $Z/\gamma^{\star}$ events are generated with the tree level matrix element generator ALPGEN [19] interfaced with the PYTHIA [20] generator for parton showering and hadronization. Diboson events are generated with PYTHIA. All simulated samples are generated using the CTEQ6L1 parton distribution functions (PDFs) [21]. The $Z/\gamma^{\star}$ samples are normalized to the NNLO cross section computed with the FEWZ program [22]. We separately simulate $Z/\gamma^{\star}$ with heavy flavor (HF) quarks, $Z/\gamma^{\star} + b\bar{b}$ (or $Z/\gamma^{\star} + c\bar{c}$), using ALPGEN and enhance the corresponding leading order cross sections by a factor estimated with the MCFM program [23]. The diboson samples are normalized to the next-to-leading order cross section calculated with MCFM. Uncertainties in these normalization factors are taken into account as systematic uncertainties. In addition, we apply a correction to the $Z/\gamma^{\star} + $ jets simulation based on data to address the imperfect modeling of the Z boson p_T in the MC [24].

The instrumental background is estimated directly from data. In the ee and $e\mu$ channels we determine the contribution of events with jets misidentified as electrons using the signal data sample but without the electron likelihood discriminant requirement. We extract the number of events with jets misidentified as electrons, n_f, and the number of events with real electrons, n_e, by maximizing the function of the electron likelihood distribution

$$\mathcal{L} = \prod_{i=1}^{N} \left[n_e S(x_i) + n_f B(x_i) \right] \frac{e^{-(n_e + n_f)}}{N!}, \tag{1}$$

where N is the number of selected events, x_i is the electron likelihood discriminant value in the event i, and $S(x_i)$ and $B(x_i)$ are the signal and background probability density functions (pdfs). The signal pdf is measured in $Z/\gamma^{\star} \to ee$ data events. The background pdf is measured in $e\mu$ events with the same selection as the analysis sample but inverting the opposite sign lepton requirement (i.e., requiring leptons of the same sign) without any topological requirement but using muon with reversed isolation requirements: $E_T^{\mu,\text{iso}}/p_T^{\mu} > 0.2$ and $p_T^{\mu,\text{iso}}/p_T^{\mu} > 0.2$. The total number of events with a jet misidentified as an electron is given by n_f scaled for the integral of $B(x)$ over the region satisfying the likelihood requirement. The estimation is performed separately in the CC and EC. We find that the contribution of instrumental background to the ee channel is negligible. The limited size of the sample used to measure the background pdf is the main contribution to the systematic uncertainty on the instrumental background. Together with a possible p_T dependence of the signal and background pdfs, these sources typically lead to systematic uncertainties of about 50%.

We also determine the number of events with an isolated muon arising from jets in the $e\mu$ and $\mu\mu$ channels. This number is estimated as $n_f^{\mu} = N_{\text{loose}} f_{\mu}$, where N_{loose} is the number of events in the same sign sample with loose isolation criteria on the muon: $E_T^{\mu,\text{iso}}/p_T^{\mu} < 0.5$ and $p_T^{\mu,\text{iso}}/p_T^{\mu} < 0.5$, and f_{μ} is the misidentification rate for isolated muons. In the $\mu\mu$ final state, we apply these loose isolation criteria only to one randomly chosen muon. In the $e\mu$ channel, the number of events with jets misidentified as electrons in the same sign sample is subtracted from N_{loose}. The misidentification rate, f_{μ}, is determined in a dimuon sample with at least one jet. In this sample we require one muon to be close to the jet ($R(\mu, \text{jet}) < 0.5$) with reversed isolation criteria $E_T^{\mu,\text{iso}}/p_T^{\mu} > 0.15$ and $p_T^{\mu,\text{iso}}/p_T^{\mu} > 0.15$. The other muon defined as the probe, should pass the loose isolation criteria $E_T^{\mu,\text{iso}}/p_T^{\mu} < 0.5$ and $p_T^{\mu,\text{iso}}/p_T^{\mu} < 0.5$. We compute f_{μ} as the ratio of the number of events in which the probe muon passes the tight isolation criteria to the total number of events in this same sign sample. The systematic uncertainty on the f_{μ} determination is about 10% and results mainly from the statistical uncertainty due to the limited size of the sample used for the muon misidentification rate calculation and the potential dependence of the misidentification rate on p_T and $\not{p}_T$.

The number of predicted background events as well as the expected number of signal events in the four channels are shown in Table 1. The $t\bar{t}$ events have two b quark jets in the final state, but most of the background events have jets produced by light quarks or gluons. In order to achieve a better separation between signal and background when measuring the cross section, we use the distribution of the smallest of the two b-tagging NN discriminants of the two leading jets. If a jet does not satisfy the requirements to enter the NN computation (non-taggable jet), a value of -1 is assigned to it. These NN discriminant distributions for the different channels are shown in Fig. 1.

We measure the $t\bar{t}$ cross section $\sigma_{t\bar{t}}$ by simultaneously fitting the NN distributions in the four channels and maximizing the likelihood function

$$\mathcal{L} = \prod_i \prod_j P\left[n_{ij}, \mu_{ij}(\sigma_{t\bar{t}}) \right], \tag{2}$$

where i runs over the channels and j over the bins of the NN distribution, and $P[n, \mu(\sigma_{t\bar{t}})]$ is the Poisson probability function to observe n events when $\mu(\sigma_{t\bar{t}})$ events are expected.

4. Results and uncertainties

The main systematic uncertainties for the measurement of the $t\bar{t}$ cross section are described in the following. A 6.1% uncertainty [14] directly affects the cross section measurement because of the luminosity uncertainty but also the expected numbers of $Z/\gamma^{\star}$ and diboson background events. Uncertainties in lepton identification efficiencies are determined by evaluating possible sources of bias in the data driven method used for the efficiency measurements and the possible impact of data/MC differences in $Z/\gamma^{\star} \to \ell\ell$ events. Uncertainties in the lepton energy resolution are determined by comparing the width of the Z boson invariant mass distributions in data and MC.

The uncertainty in the relative JES between data and MC for light quark jets has been evaluated by shifting the jets in MC by their corresponding JES uncertainty. The uncertainty on the difference between the light and b quark JES (1.8%) is estimated by propagating the difference in the single pion response between data and MC to the MC JES for b quark jets. Jet energy resolution uncertainties are estimated by comparing the resolutions

Table 1

Numbers of expected and observed events assuming the SM $t\bar{t}$ cross section for a top quark mass of $m_t = 172.5$ GeV (7.45 pb). Expected numbers of events are shown with their systematic uncertainties. The uncertainty on the ratio between observed and expected numbers of events takes into account the statistical uncertainty in the observed number of events (N_{obs}) and the systematic uncertainty in the expected number of events (N_{exp}).

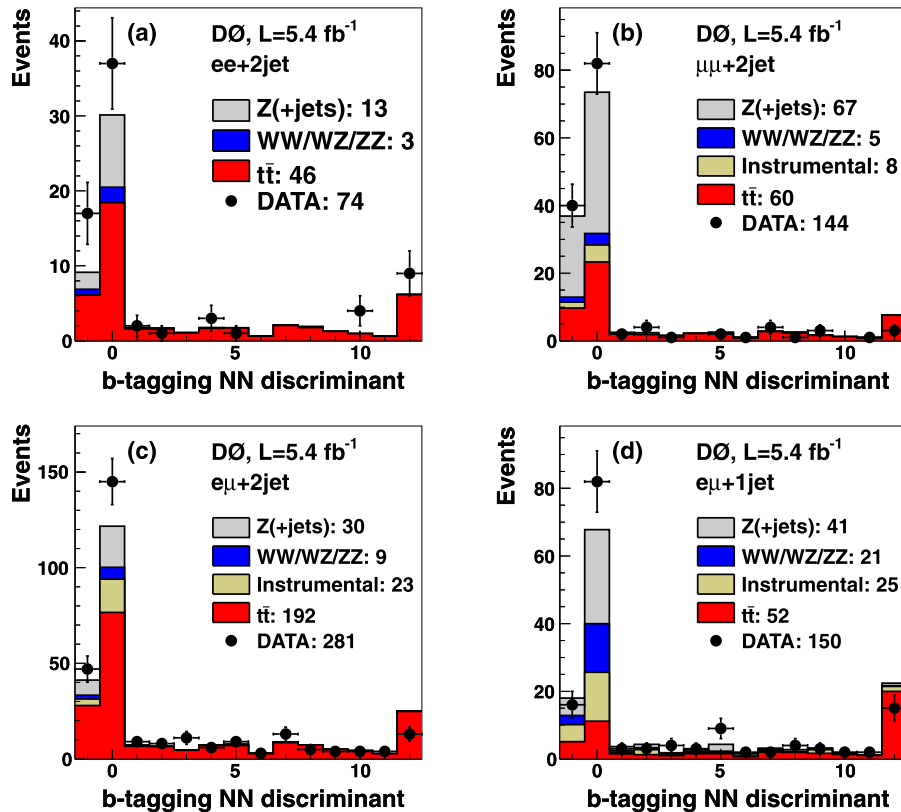| Channel	$Z \to \ell\ell$	Diboson	Instrumental background	$t\bar{t} \to \ell\bar{\ell}b\bar{b}\nu\bar{\nu}$	N_{exp}	N_{obs}	$\frac{\text{Observed}}{\text{Expected}}$
$ee + 2$jet	12.6 ± 2.0	3.0 ± 0.4	–	45.6 ± 5.3	61.1 ± 7.1	74	1.21 ± 0.20
$\mu\mu + 2$jet	67.3 ± 9.7	5.1 ± 0.7	7.6 ± 1.2	59.8 ± 6.6	139.8 ± 15.7	144	1.03 ± 0.14
$e\mu + 2$jet	30.3 ± 4.2	8.6 ± 1.2	22.7 ± 8.6	191.5 ± 18.8	253.1 ± 24.3	281	1.11 ± 0.13
$e\mu + 1$jet	40.9 ± 4.8	20.7 ± 2.4	25.3 ± 10.5	52.1 ± 9.4	139.0 ± 16.5	150	1.08 ± 0.16

Fig. 1. Expected and observed distributions for the smallest *b*-tagging NN discriminant output of the two leading jets for the (a) $ee + 2$ jet channel, (b) $\mu\mu + 2$ jet channel, (c) $e\mu + 2$ jet channel, and (d) $e\mu + 1$ jet channel. The $t\bar{t}$ signal is normalized to the SM cross section (7.45 pb). The *x* axis represents the NN output non-uniformly mapped to 14 bins. The bin with central value 0 represents the lowest probability for a jet to be produced by a *b* quark. The bin with value 12 represents the highest probability. The bin with value −1 represents the jets which do not satisfy the requirements to enter the NN computation (non-taggable jets).

measured in $Z/\gamma^* +$ jets events in data and in MC. The uncertainty on the jet identification efficiency is estimated by comparing the efficiencies measured in dijet events for data and MC. The *b* quark identification uncertainties include uncertainties in the probability of tagging a *b* quark jet, the probability of tagging a light quark jet or gluon, and the probability for a jet not to be taggable [17].

To estimate the uncertainty in the trigger efficiency, we use events selected with the same criteria as the $t\bar{t}$ signal but without jet requirements. In all four channels this selection is dominated by Z/γ^* events. We compute the ratio of the expected and observed number of events for two cases: when both leptons are allowed to fire the trigger or when only one lepton is allowed to fire the trigger. The difference in these ratios is used to estimate the uncertainty on the trigger efficiency.

Several uncertainties on the signal modeling are considered. The effects of higher order corrections and the hadronization modeling are estimated as the difference in signal efficiencies using the default ALPGEN + PYTHIA simulation and using events generated with the MC@NLO [25] + HERWIG [26] simulation. The uncertainty coming from color reconnection is evaluated by comparing the

$t\bar{t}$ efficiency using PYTHIA v6.4 tune Apro and PYTHIA v6.4 tune ACRpro [27]. The uncertainty on initial (ISR) and final (FSR) state radiation is evaluated by varying the ISR/FSR parameters in PYTHIA up to 20% and evaluating the change in the signal efficiency. The uncertainty due to PDFs is estimated by reweighting the signal efficiency to the CTEQ6.1M PDFs [21] and looking at the efficiency variation for each eigenvector set that define the CTEQ6.1M uncertainty range. The uncertainty due to the simulation of *b* quark fragmentation is assigned to be the difference between tuning the parameters of the *b* quark fragmentation function to LEP or SLD data [28].

The uncertainty in the background normalization includes the theoretical uncertainties in the cross section and the uncertainty due to the correction for the *Z* boson p_T modeling. We also take into account an uncertainty due to the limited statistics of the signal and background templates of the NN discriminant. For the following systematic uncertainties, we take into account effects that change the shape of the differential distribution of the *b*-tagging NN output discriminant: jet energy scale, jet resolution, jet identification, and *b* quark identification uncertainties.

Table 2

Breakdown of uncertainties on the $t\bar{t}$ cross sections in the $\ell\ell'$ channel and for the combined $\ell\ell'$ and ℓj measurement using the nuisance parameter technique. The $\pm\sigma$ give the impact on the measured cross section when the nuisance parameters describing the considered category are shifted by ±1 SD from their fitted mean. See text for further details.

Source	$\ell\ell'$		$\ell\ell' + \ell j$	
	$+\sigma$ [pb]	$-\sigma$ [pb]	$+\sigma$ [pb]	$-\sigma$ [pb]
Statistical	+0.50	−0.48	+0.20	−0.20
Muon identification	+0.11	−0.11	+0.07	−0.06
Electron identification and smearing	+0.24	−0.23	+0.13	−0.13
Signal modeling	+0.34	−0.33	+0.16	−0.06
Triggers	+0.19	−0.19	+0.05	−0.05
Jet energy scale	+0.13	−0.12	+0.04	−0.04
Jet reconstruction and identification	+0.21	−0.20	+0.12	−0.09
b-tagging	+0.06	−0.06	+0.16	−0.14
Background normalization	+0.29	−0.27	+0.11	−0.10
$W + $ HF fraction	–	–	+0.12	−0.04
Instrumental background	+0.18	−0.17	+0.05	−0.04
Luminosity	+0.57	−0.51	+0.48	−0.43
Other	+0.10	−0.10	+0.06	−0.06
Template statistics	+0.08	−0.08	+0.04	−0.04

Maximizing the likelihood function in Eq. (2) and using the above systematic uncertainties, we measure the cross section assuming a top quark mass $m_t = 172.5$ GeV and find

$$\sigma_{t\bar{t}} = 8.05^{+0.50}_{-0.48}(\text{stat})^{+1.05}_{-0.97}(\text{syst}) \text{ pb}. \quad (3)$$

In order to reduce the influence of systematic uncertainties on the cross section measurement, in the following we use nuisance parameters [29] to constrain the overall uncertainty using the data NN output distribution itself. Using this technique, the likelihood (Eq. (2)) is modified,

$$\mathcal{L} = \prod_i \prod_j P\big[n_{ij}, \mu_{ij}(\sigma_{t\bar{t}}, \nu_k)\big] \prod_k \mathcal{G}(\nu_k; 0, \text{SD}), \quad (4)$$

where $\mathcal{G}(\nu_k; 0, \text{SD})$ denotes the Gaussian probability density with mean at zero and width corresponding to one standard deviation (SD) of the considered systematic uncertainty. Correlations of systematic uncertainties between channels and between the different samples are naturally taken into account by assigning the same nuisance parameter to the correlated systematic uncertainties. In Eq. (4), the free parameters of the fit are ν_k and $\sigma_{t\bar{t}}$.

As can be seen from Eq. (3), the systematic uncertainties are the limiting uncertainties in the precision of the $t\bar{t}$ cross section measurement. Varying the systematic uncertainties and constraining them with data can therefore improve the measurement. Using nuisance parameters we find an overall improvement of the uncertainty of 20% and reach a relative precision of 11% in the $t\bar{t}$ cross section:

$$\sigma_{t\bar{t}} = 7.36^{+0.90}_{-0.79}(\text{stat} + \text{syst}) \text{ pb}.$$

The uncertainties on the $t\bar{t}$ cross section are summarized in Table 2. For each category of systematic uncertainty listed in Table 2, the corresponding nuisance parameters are set to their fitted value, and shifted by the uncertainty on the fit. In the columns "$+\sigma$" and "$-\sigma$," the positive and negative systematic uncertainties on the measured cross section for each category are listed.

We combine this measurement with the cross section measurement in the non-overlapping ℓj channel [6] using the same nuisance parameter approach and taking correlations between common systematics uncertainties into account. In the ℓj channel, the events are separated into events with three or at least four jets, of which zero, one, or at least two jets are b-tagged. In events that have three or four jets but no b-tagged jets or events with

three jets and one b-tagged jet, we use a topological discriminant to improve the separation of signal and background. In [6], the separation into these channels and application of topological methods is referred to as the combined method. For this combination, we do not simultaneously fit the heavy flavor fraction for $W + $ jet processes ($W + $ HF) in the ℓj channel as was done in [6], making it unnecessary to use ℓj events with only two jets. With this change compared to [6], the measured ℓj $t\bar{t}$ cross section is

$$\sigma_{t\bar{t}} = 7.90^{+0.78}_{-0.69}(\text{stat} + \text{syst}) \text{ pb}.$$

The combination of the measurements in the dilepton and lepton + jet final states is done by maximizing the product of the likelihood function for the $\ell\ell'$ and ℓj channels, which yields

$$\sigma_{t\bar{t}} = 7.56^{+0.63}_{-0.56}(\text{stat} + \text{syst}) \text{ pb}$$

for $m_t = 172.5$ GeV. This combination has a relative precision of 8% and represents an improvement of about 12% relative to the ℓj cross section measurement alone. The uncertainties for this combined measurement are summarized in Table 2.

Due to acceptance effects, the $t\bar{t}$ efficiency depends on the assumed m_t in the MC. We extract the $t\bar{t}$ cross section using simulated $t\bar{t}$ events with different values of m_t. The resulting cross sections can be fitted with the following functional form:

$$\sigma_{t\bar{t}}(m_t) = \frac{1}{m_t^4}\big[a + b(m_t - 170 \text{ GeV})$$
$$+ c(m_t - 170 \text{ GeV})^2 + d(m_t - 170 \text{ GeV})^3\big], \quad (5)$$

with $a = 6.5178 \times 10^9$ GeV^4, $b = 7.884 \times 10^7$ GeV^3, $c = 9.3069 \times 10^5$ GeV^2, and $d = -2.42 \times 10^3$ GeV and where $\sigma_{t\bar{t}}$ and m_t are in pb and GeV, respectively. The relative uncertainty on the cross section for different mass points is the same as the one obtained for $m_t = 172.5$ GeV. Fig. 2 shows this parameterization for the measurement as a function of top quark mass together with approximate NNLO computations [1–3].

5. Conclusion

In this Letter we presented an updated measurement of the $t\bar{t}$ production cross section in the dilepton final state using 5.4 fb^{-1} of integrated luminosity. This cross section measurement yields $\sigma_{t\bar{t}} = 7.36^{+0.90}_{-0.79}(\text{stat} + \text{syst})$ pb and has a relative precision of $^{+12\%}_{-11\%}$. It is currently the most precise measurement of the $t\bar{t}$ cross section
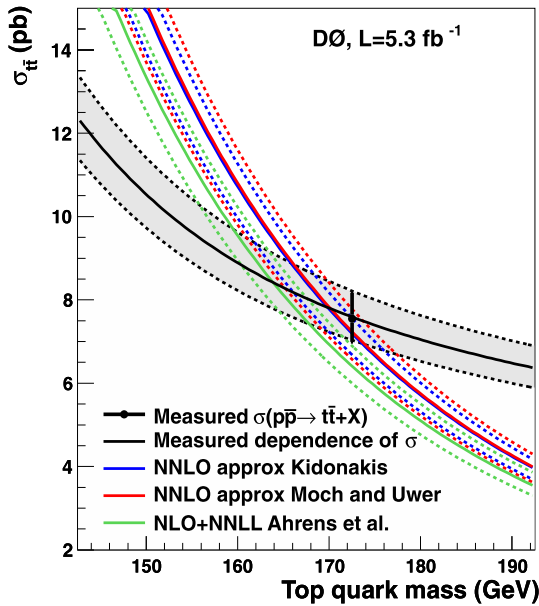
Fig. 2. Dependence of the experimental and theoretical [1–3] $t\bar{t}$ cross sections on the top quark mass. The colored dashed lines represent the uncertainties for all three theoretical calculations from the choice of the PDF and the renormalization and factorization scales (added quadratically). The data point shows the combined $\ell\ell'$ and ℓj cross section measurement for $m_t = 172.5$ GeV, the black curve is experimental $t\bar{t}$ cross section as a function of m_t, and the gray band corresponds to the total experimental uncertainty.

in the dilepton channel. Combining this measurement with our result in the lepton + jets channel [6] yields $7.56^{+0.63}_{-0.56}$ (stat + syst) pb which corresponds to a relative precision of 8%. This measurement is in good agreement with the SM prediction.

Acknowledgements

References

[1] V. Ahrens, A. Ferroglia, M. Neubert, B.D. Pecjak, L.L. Yang, J. High Energy Phys. 1009 (2010) 097;
V. Ahrens, A. Ferroglia, M. Neubert, B.D. Pecjak, L.L. Yang, Nucl. Phys. B (Proc. Suppl.) 205–206 (2010) 48.
[2] S. Moch, P. Uwer, Phys. Rev. D 78 (2008) 034003;
U. Langenfeld, S. Moch, P. Uwer, Phys. Rev. D 80 (2009) 054009.
[3] N. Kidonakis, R. Vogt, Phys. Rev. D 68 (2003) 114014;
N. Kidonakis, Phys. Rev. D 82 (2010) 114030.
[4] V.M. Abazov, et al., D0 Collaboration, Phys. Lett. B 679 (2009) 177.
[5] V.M. Abazov, et al., D0 Collaboration, Phys. Rev. D 80 (2009) 071102.
[6] V.M. Abazov, et al., D0 Collaboration, Phys. Rev. D 84 (2011) 012008.
[7] V.M. Abazov, et al., D0 Collaboration, Phys. Rev. Lett. 100 (2008) 192004.
[8] V.M. Abazov, et al., D0 Collaboration, Phys. Rev. D 76 (2007) 072007;
V.M. Abazov, et al., D0 Collaboration, Phys. Rev. D 82 (2010) 032002.
[9] V.M. Abazov, et al., D0 Collaboration, Phys. Lett. B 626 (2005) 55.
[10] T. Aaltonen, et al., CDF Collaboration, Phys. Rev. D 82 (2010) 052002.
[11] G. Aad, et al., ATLAS Collaboration, Eur. Phys. J. C 71 (2011) 1577.
[12] V. Khachatryan, et al., CMS Collaboration, Phys. Lett. B 695 (2011) 424.
[13] V.M. Abazov, et al., D0 Collaboration, Nucl. Instrum. Methods Phys. Res. A 565 (2006) 463.
[14] T. Andeen, et al., FERMILAB-TM-2365, 2007.
[15] R. Brun, F. Carminati, CERN Program Library Long Writeup W5013, 1993 (unpublished).
[16] G.C. Blazey, et al., in: U. Baur, R.K. Ellis, D. Zeppenfeld (Eds.), Proceedings of the Workshop: "QCD and Weak Boson Physics in Run II", Fermilab, Batavia, IL, 2000, p. 47, arXiv:hep-ex/0005012, see Section 3.5 for details.
[17] V.M. Abazov, et al., D0 Collaboration, Nucl. Instrum. Methods Phys. Res. A 620 (2010) 490.
[18] V.M. Abazov, et al., D0 Collaboration, Phys. Rev. D 76 (2007) 052006.
[19] M.L. Mangano, M. Moretti, F. Piccinini, R. Pittau, A.D. Polosa, J. High Energy Phys. 0307 (2003) 001.
[20] T. Sjöstrand, S. Mrenna, P.Z. Skands, J. High Energy Phys. 0605 (2006) 026.
[21] P.M. Nadolsky, et al., Phys. Rev. D 78 (2008) 013004.
[22] R. Gavin, Y. Li, F. Petriello, S. Quackenbush, arXiv:1011.3540 [hep-ph].
[23] R.K. Ellis, Nucl. Phys. B (Proc. Suppl.) 160 (2006) 170.
[24] V.M. Abazov, et al., D0 Collaboration, Phys. Lett. B 693 (2010) 522.
[25] S. Frixione, B.R. Webber, JHEP 0206 (2002) 029, arXiv:hep-ph/0204244;
S. Frixione, P. Nason, B.R. Webber, JHEP 0308 (2003) 007, arXiv:hep-ph/0305252.
[26] G. Corcella, I.G. Knowles, G. Marchesini, S. Moretti, K. Odagiri, P. Richardson, M.H. Seymour, B.R. Webber, J. High Energy Phys. 0101 (2001) 010.
[27] A. Buckley, H. Hoeth, H. Lacker, H. Schulz, J.E. von Seggern, Eur. Phys. J. C 65 (2010) 331;
P.Z. Skands, D. Wicke, Eur. Phys. J. C 52 (2007) 133.
[28] Y. Peters, K. Hamacher, D. Wicke, FERMILAB-TM-2425-E.
[29] P. Sinervo, in: L. Lyons, R. Mount, R. Reitmeyer (Eds.), Proceedings of PHYSTAT 2003: "Statistical Problems in Particle Physics, Astrophysics, and Cosmology", SLAC, Menlo Park, CA, 2003, p. 122, SLAC-R-703.